A $Sc_{0.2}Al_{0.8}N$-based 14 GHz Film Bulk Acoustic Resonator with over 8% Coupling Coefficient and over 400 Quality factor for Ku-band applications

Chen Liu
Institute of Microelectronics
*Agency for Science, Technology and Research (A*STAR)*
Singapore
liuc@ime.a-star.edu.sg

Xinghua Wang
Institute of Microelectronics
*Agency for Science, Technology and Research (A*STAR)*
Singapore
Wang_Xinghua@ime.a-star.edu.sg

Wenjia Yang
Institute of Microelectronics
*Agency for Science, Technology and Research (A*STAR)*
Singapore
Yang_Wenjia@ime.a-star.edu.sg

Ying Zhang
Institute of Microelectronics
*Agency for Science, Technology and Research (A*STAR)*
Singapore
zhang_ying@ime.a-star.edu.sg

Eugene Yi Zhun Woo
Institute of Microelectronics
*Agency for Science, Technology and Research (A*STAR)*
Singapore

Yao Zhu
Institute of Microelectronics
*Agency for Science, Technology and Research (A*STAR)*
Singapore
zhuya@ime.a-star.edu.sg

***Abstract* — It's challenging to scale down the stack of the acoustic resonator to achieve high frequency like >8 GHz, because of the low crystallinity of the thin piezoelectric film and large parasitics in ultrathin electrode layers. In this work, film bulk acoustic resonator (FBAR) devices based on 90 nm 20% Sc doped AlN ($Sc_{0.2}Al_{0.8}N$) film have been fabricated and characterized. High-quality thin ScAlN film without obvious interfacial layer and abnormal grains has been achieved. The de-embedded testing results show that the demonstrated resonator has achieved over 14 GHz frequency with a Q factor of over 400 and an effective coupling coefficient of over 8%, which is promising for Ku-band filtering applications.**

Keywords—Piezoelectric, bulk acoustic wave, resonator, Ku-band

I. INTRODUCTION

Acoustic resonators and filters are key components in current wireless communication systems, due to their high quality factor, low insertion loss and small chip size. Since the sub-6 GHz Radio Frequency (RF) spectrum is becoming congested, the demand for acoustic filters to support higher frequencies increases with the development of advanced 5G and future 6G technologies. Although film bulk acoustic resonator (FBAR) technology has commercially dominated the <6 GHz frequency range, it's quite challenging to scale down the stack to achieve higher frequencies like >10 GHz, because of the low crystallinity of the thin piezoelectric film and large parasitics in ultrathin electrode layers.

In this work, FBAR devices with 90 nm $Sc_{0.2}Al_{0.8}N$ film were fabricated achieving over 14 GHz frequency, along with high quality factor over 400. By de-embedding the parasitic resistance and inductance, the intrinsic resonator performance has been unveiled for detecting the resonant frequency, the effective coupling coefficient, and the extraction of c33 and e33 of the piezoelectric ScAlN film. With a high effective coupling coefficient of over 8% and Q factor of over 400, the demonstrated FBAR resonators are promising for the filtering applications in the Ku-band (12-18 GHz) of the 5G technology.

II. FABRICATION AND FILM CHARACTERIZATION

A. Device fabrication

Fig. 1 (a) shows the optical micrograph of the fabricated FBAR test structure. A large ground-signal-ground (GSG) periphery structure has been implemented for the auto-testing of a wide range of FBAR areas from ~100 μm^2 to ~ 10^4 μm^2. Fig. 1 (b) is the zoom-in view of the core FBAR device, including the swimming pool and the release hole for the underneath cavity. The lateral dimension of the polygon is designed to be 10 – 20 µm, and the radius of the release hole is 3 µm. Fig. 1 (c) is the schematical cross-section of the dashed line marked in Fig. 2 (b). The process generally follows our previous flow for the GHz RFMEMS resonators and filters [1][2], with an Al_2O_3 passivated swimming pool for the cavity beneath the FBAR stack. For the designed thin stack of Mo (40 nm)/$Sc_{0.2}Al_{0.8}N$ (90 nm)/ Mo (50 nm), to avoid the vaper HF leak through the ScAlN region without top and bottom electrode, global passivation is introduced to cover the top surface of the wafer, and then the pad regions were etched to expose the Al for contacting. Etching of this global passivation layer can also tune the resonant frequency of the FBAR to construct a ladder filter.

B. Film characterization

The key of an FBAR resonator for over 10 GHz with an ultrathin regime is the quality of the ~100 nm piezoelectric film. In the presented devices, the 90 nm thick $Sc_{0.2}Al_{0.8}N$ film was deposited by a single 300 mm target sputtering with an optimized recipe on a 200 mm wafer. Before the deposition of this 90 nm film, a 20 nm seed layer along with the 50 nm bottom Mo electrode layer was deposited first. Fig. 2 (a) shows the cross-sectional TEM image of the FBAR stack with highlighted thickness for each layer. One general challenge in the PVD ScAlN deposition technology is the existence of abnormal grains [3]. From this cross-section, no abnormal grains are found in the deposited $Sc_{0.2}Al_{0.8}N$ films. Zoom-in views of the top interface, bulk, and bottom interface of the ScAlN layer are shown in Fig. 2 (b), (c) & (d), respectively. For the top interface with Molybdenum, the surface of the ScAlN film is quite smooth, and the oxidation layer between the ScAlN and Molybdenum is nearly undetectable. The texture of the film is uniform from the bottom to the top surface of the ScAlN film. The starting amorphous layer is only 2 – 3 nm thick in the deposited thin ScAlN layer. The high-quality thin $Sc_{0.2}Al_{0.8}N$ enables low mechanical damping and a high-quality factor for the over 10 GHz acoustic resonator.

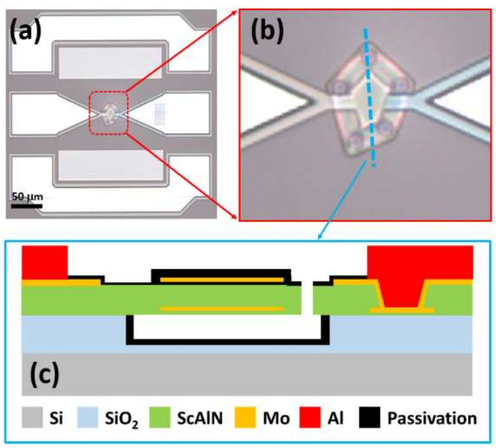

Fig. 1. Fabrication results of the demonstrated FBAR device. (a) Optical micrograph and (b) Zoom-in view of the fabricated FBAR device with GSG testing structures. (c) Schematical cross-section of the fabricated FBAR device.

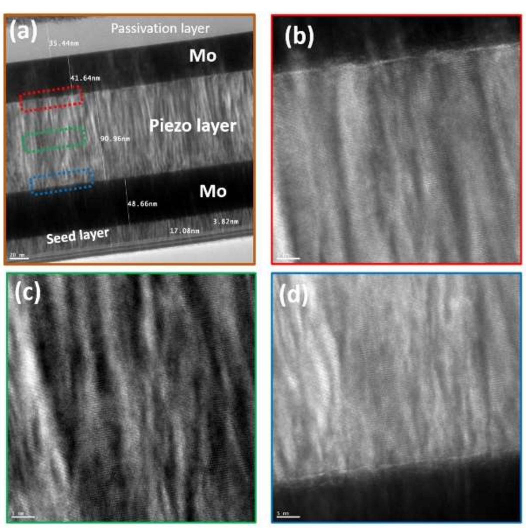

Fig. 2. Cross-sectional TEM images of (a) Whole FBAR stack; (b) Zoom-in view of the interface between the top electrode and ScAlN layer; (c) Zoom-in view of the bulk of the ScAlN layer; (d) Zoom-in view of the interface between the bottom electrode and ScAlN layer.

III. Measurements and Discussion

A. Measurement

The 2-port and 50 Ω loaded S-parameter testing of the fabricated resonators was performed with a Keysignt N5244B PNA-X Microwave Network Analyzer. The test structure is shown in Fig. 1 (a), including the resonator and the GSG surroundings. The spectrum of the magnitude and phase of the impedance from 13 GHz to 17 GHz are derived from the measured s2p results, as shown in Fig. 3 (a). From the magnitude spectrum, the anti-resonant frequency (f_p) with maximum impedance is clearly observed at the expected frequency range, while resonant frequency (f_s) with minimum impedance is not obvious due to the high resistance of the ultrathin (40 nm) Mo layer. From the measured phase of the impedance, at the off-resonance frequency range, the phase is above 0, instead of $-\pi/2$ for an ideal FBAR resonator, which can be treated as a capacitor at the off-resonance. This positive phase indicates the existence of an unexpected series inductance in the test structure, which may originate from the GSG surroundings. Since the impedance of an inductor is increasing with the frequency, the impact of this parasitic inductance becomes more significant in the ~ 15 GHz frequency compared to the ~5 GHz frequency. The quality factor (Q) of the fabricated resonator is derived from the measured s-parameter (2-port transferred to 1-port) with the Bode equation as below:

$$Q(f) = 2\pi f \cdot \tau(f) \cdot mag(S11)/(1-mag(S11)^{2})$$

The curve of the Q spectrum is shown in Fig. 3 (b). Due to the series parasitics, the Q at f_s (Q_s) is less than 100, while the Q_p is over 400.

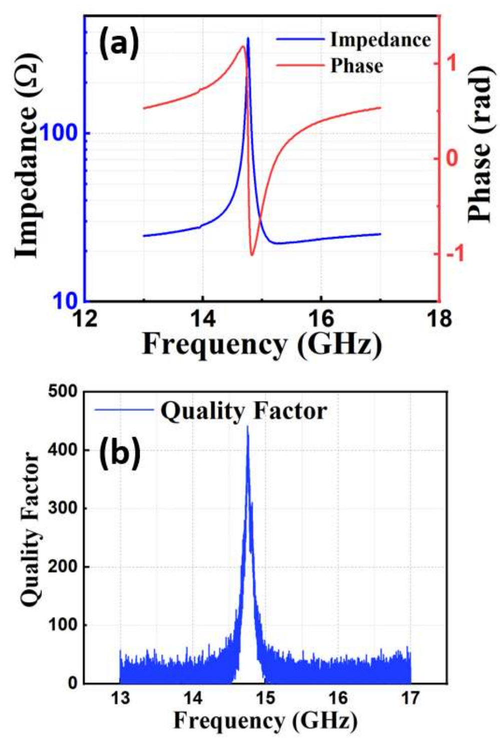

Fig. 3. Measurement results of the fabricated FBAR. (a) Impedance and phase spectrum. (b) Calculated Bode Q factor from the measurement S parameter.

B. De-embedding

De-embedding of the FBAR testing structures is necessary for the over 10 GHz resonators to unveil the intrinsic response of the resonator. There are several methods to de-embedded the parasitics, in this work, the Open-Short-Through de-embedding is utilized with measurements of the open, short, and through test structures, respectively [4]. The de-embedded magnitude and phase of the impedance are shown in Fig. 4 (a) and (b). By de-embedding the series resistance and the inductance, the fs can be identified at ~ 14.25 GHz, with nearly no shift of the f_p in the measurement. The effective coupling coefficient (k^2_{eff}) can be calculated as 8.5% with the following equation:

$$k^2_{eff} = \theta/\tan(\theta),\ \theta = (\pi/2)(f_s/f_p)$$

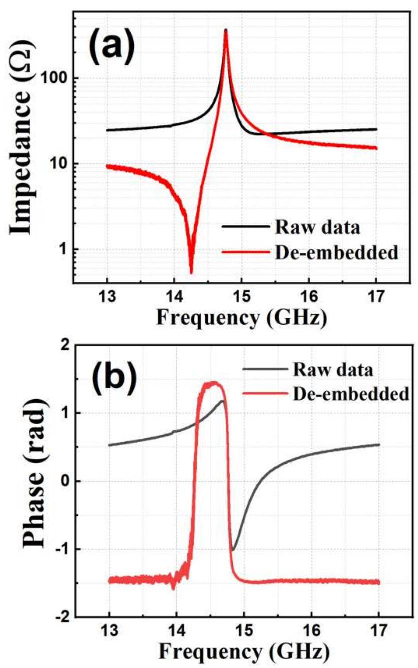

Fig. 4. Comparison of raw data and de-embedded results (a) the magnitude of the impedance; (b) the phase of the impedance.

C. Film properties extraction

The de-embedded resonator impedance spectrum, along with the finite element modeling (FEM), can be utilized to extract the FBAR-related material properties of the deposited thin $Sc_{0.2}Al_{0.8}N$ film, including the longitudinal elasticity (c33) and the piezoelectric coupling coefficient (e33) along the thickness axis [5]. The geometry model was built according to the cross-sectional TEM image of the FBAR stack with a measured thickness for each layer. The mechanical properties of the Mo, passivation layer, and seed layer are predefined with the COMSOL library materials. The dielectric constant (ε) was extracted by measuring the capacitance of the plate capacitor. The fs of the FEM simulation results are linearly fitted with the preset sweeping c33, as shown in Fig. 5 (a). By matching the fs from the de-embedded impedance plot, the c33 can be extracted as 279 ± 2 GPa. As shown in Fig. 5 (b), with similar simulations, the e33 can be extracted from the linear fitting curve of fp/fs with sweeping e33, to be 1.99 ± 0.21 C/m². The c33 is comparable with the value of thick $Sc_{0.2}Al_{0.8}N$ film with a thickness of 1 μm, while the e33 is slightly smaller than the theoretical value (>2 C/m²) for the 20% Sc dopant. The comparison between the de-embedded and the simulated impedance spectrum is shown in Fig. 5 (c).

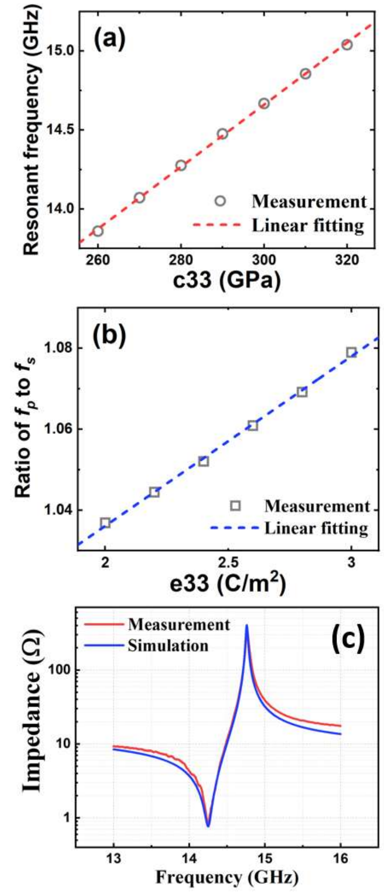

Fig. 5. Material properties extraction by FEM. (a) Linear fitting of c_{33} with f_s; (b) Linear fitting of e_{33} with f_p/f_s; (c) Comparison of measurement and simulation.

D. Benchmark

The demonstrated 15 GHz resonator has been compared with the other AlN or ScAlN-based acoustic resonators for over 8 GHz applications, as shown in Fig. 6 [6-13]. Besides the resonant frequency, another two key parameters for the filtering applications are the k^2_{eff} and Q, determining the bandwidth and the roll-off & the insertion loss of the filter, respectively. Thus, a figure of merit of the resonator can be defined as FOM = k^2_{eff} * Q. It should be noted that the piezoelectric thin film quality is naturally worse compared to thick films with ~ 1 μm thickness for the PVD deposited ScAlN, making it challenging to achieve both high Q and k^2_{eff} for high-frequency resonators over 8 GHz. The benchmarks of the Q factor, k^2_{eff}, and the FOM are shown in Fig. 6 (a), (b), and (c). For the FBAR resonator demonstrated in this work, both the Q factor and the k^2_{eff} are among the first tier, leading to the highest FOM. Optimization of the resistivity of the thin electrode layer and the deposition recipe is necessary for further development of the acoustic filters in the over 8 GHz frequency range.

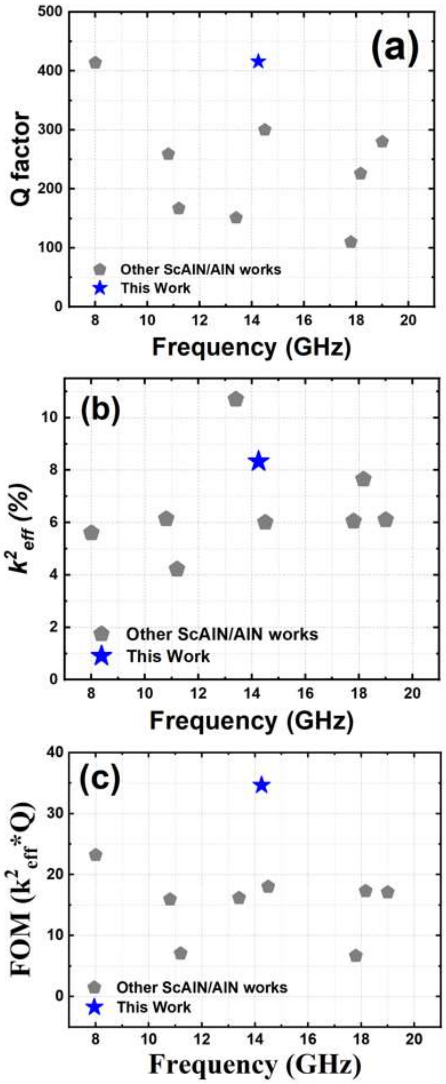

Fig. 7. Benchmark of the demonstrated AlN or ScAlN-based resonators for over 8 GHz frequency [6-13]. (a) Comparison of Q factor. (b) Comparison of k^2_{eff}. (c) Comparison of figure of merit (K^2_{eff}*Q).

IV. Conclusion

This work presents FBAR devices with resonant frequency of over 14 GHz for Ku-band filtering applications. The resonators were fabricated based on high-quality 200 mm 90 nm $Sc_{0.2}Al_{0.8}N$ film sandwiched between 40 nm & 50 nm Mo electrodes, achieving a high-quality factor over 400. By de-embedding the parasitics from the periphery structures of the resonator, the intrinsic resonant frequency, effective coupling coefficient, and the material parameters of the piezoelectric ScAlN film are derived and extracted. With a high effective coupling coefficient of over 8% and Q factor of over 400, the demonstrated FBAR resonators are promising for the filtering applications in the Ku-band (12-18 GHz) of the 5G technology.

Acknowledgment

This work was supported by the Science and Engineering Research Council of A*STAR (Agency for Science, Technology and Research), Singapore, under Grant no (A20G9b0135).

References

[1] N. Wang, Yao Zhu, Geng Li Chua, Bangtao Chen, Srinivas Merugu, Navab Sing and Yuandong Gu, "Over 10% of k2eff Demonstrated by 2-GHz Spurious Mode-Free Sc0.12Al0.88N Laterally Coupled Alternating Thickness Mode Resonators," IEEE Electron Device Letters, vol. 40, pp. 957-960, 2019

[2] Y. Zhu, Nan Wang, Chengliang Sun, Srinivas Merugu, Navab Singh, and Yuandong Gu, "A High Coupling Coefficient 2.3-GHz AlN Resonator for High Band LTE Filtering Application," IEEE Electron Device Letters, vol. 37, pp. 1344- 1346, 2016

[3] M. Li, K. Hu, H. Lin, and Y. Zhu, "Structural characterization of the abnormal grains evolution in sputtered ScAlN films," *IEEE Int. Ultrason. Symp. IUS*, pp. 1–3, 2021, doi: 10.1109/IUS52206.2021.9593514.

[4] Errikos Lourandakis, On-Wafer Microwave Measurements and De-embedding. Artech House

[5] C. Liu, Y. Zhang, N. Wang, and Y. Zhu, "Material Parameter Extraction Method for SCxAl1-xN Films Using Multiple Linear Regression and Wafer-level Uniformity Analysis," *IEEE Int. Ultrason. Symp. IUS*, vol. 2022-Octob.

[6] Izhar, M. M. A. Fiagbenu, P. Musavigharavi, X. Du, J. Leathersich, et al., "A K-Band Bulk Acoustic Wave Resonator Using Periodically Poled Al0.72Sc0.28N," in IEEE Electron Device Letters, vol. 44, no. 7, pp. 1196-1199, July 2023

[7] M. Park, Z. Hao, R. Dargis, A. Clark, and A. Ansari, "Epitaxial Aluminum Scandium Nitride Super High Frequency Acoustic Resonators," *J. Microelectromechanical Syst.*, vol. 29, no. 4, pp. 490–498, 2020.

[8] M. Assylbekova, G. Chen, M. Pirro, G. Michetti, and M. Rinaldi, "Aluminum Nitride Combined Overtone Resonator for Millimeter Wave 5g Applications," Proc. IEEE Int. Conf. Micro Electro Mech. Syst., vol. 2021-Janua, no. January, pp. 202–205, 2021.

[9] M. Assylbekova, G. Chen, G. Michetti, M. Pirro, L. Colombo, and M. Rinaldi, "11 GHz Lateral-Field-Excited Aluminum Nitride Cross-Sectional Lamé Mode Resonator," IFCS-ISAF 2020 - Jt. Conf. IEEE Int. Freq. Control Symp. IEEE Int. Symp. Appl. Ferroelectr. Proc., pp. 4–7, 2020.

[10] M. Hara et al., "Super-high-frequency band filters configured with air-gap-type thin-film bulk acoustic resonators," Jpn. J. Appl. Phys., vol. 49, no. 7 PART 2, 2010.

[11] K. Umeda, H. Kawamura, M. Takeuchi, and Y. Yoshino, "Characteristics of an AlN-based bulk acoustic wave resonator in the super high frequency range," Vacuum, vol. 83, no. 3, pp. 672–674, 2008.

[12] M. Park, J. Wang, and A. Ansari, "An 18 GHz AlScN Film Bulk Acoustic Wave Resonator with Epitaxial Metal Electrodes", the 22nd International Conference on Solid-State Sensors, Actuators and Microsystems (Transducers 2023)

[13] G. Giribaldi, L. Colombo, P. Simeoni, and M. Rinaldi, "Micro-to-Nanoscale ScAlN Lamb Wave Resonators; Frequency scaling towards the mmWave Spectrum", the 22nd International Conference on Solid-State Sensors, Actuators and Microsystems (Transducers 2023).